Available online at www.sciencedirect.com
ScienceDirect
Scripta Materialia 59 (2008) 239–242
Scripta MATERIALIA
www.elsevier.com/locate/scriptamat

Mechanical and electrochemical properties of laser surface nitrided Ti–6Al–4V

A. Biswas,[a] L. Li,[b] U.K. Chatterjee,[a] I. Manna,[a] S.K. Pabi[a] and J. Dutta Majumdar[a,*]

[a] *Department of Metals and Materials Engineering, Indian Institute of Technology Kharagpur, West Bengal 721 302, India*
[b] *School of Mechanical, Aerospace and Civil Engineering, University of Manchester, Manchester - M60, 1QD, UK*

Received 29 December 2007; revised 12 March 2008; accepted 15 March 2008
Available online 26 March 2008

The present study concerns laser surface nitriding of Ti–6Al–4V. The microstructure of the surface nitrided Ti–6Al–4V consisted of TiN dendrites distributed in alpha Ti matrix. The microhardness of the surface was improved to 1142 VHN as compared to the 260 VHN of substrate. The bulk modulus of the surface was increased to 177 GPA as compared to the 114 GPA of the substrate. The pitting corrosion resistance and wettability were significantly improved against simulated body fluid.

Keywords: Ti alloys; Laser treatment; Corrosion; Hardness; Biomaterials

Titanium and its alloys are widely used as aerospace components and as surgical implants because of their good corrosion resistance, their bulk modulus being comparable to that of human bone and their biocompatibility [1–3]. However, the poor wear resistance of Ti-based alloys causes restrictions in the prolonged use of Ti for bioimplants. Over the last decade, various types of surface modification techniques have been developed aimed at improving the wear resistance of Ti and its alloys [4–7]. Laser gas alloying is a technique used to modify the near-surface microstructure and/or composition by melting the surface using a high-power laser beam with reactive gas as a shrouding environment [8,9]. Laser gas alloying of Ti and Ti–6Al–4V (Ti64) alloys to form a nitride layer on the surface of Ti–6Al–4V has been extensively investigated with the aim of improving the alloy's tribological properties [9–11]. Man et al. [12] nitrided the surface of Ti–6Al–4V substrate using a continuous wave Nd:YAG laser and reported improved adhesion between the glass coating and the LGN-etched specimen as compared to a sand-blasted one. In the present study, laser surface nitriding of Ti–6Al–4V was attempted using a continuous wave diode laser. Preliminary investigations showed that laser surface nitrided Ti–6Al–4V had improved biocompatibility, and it was observed that the laser parameters influenced the microstructure and properties [13]. In the present study, the effects of laser surface nitriding of Ti–6Al–4V (under optimum conditions) on the microstructure, mechanical properties, corrosion resistance (in simulated biofluid) and wettability was investigated.

Ti–6Al–4V (Ti64) of dimensions 20 mm × 20 mm × 5 mm was chosen as the substrate. The substrate surface was sand blasted prior to laser processing to clean the surface and improve the absorptivity. Laser surface nitriding was carried out by irradiating the substrate using a 2 kW continuous wave (CW) Laserline diode laser with mixed 810 and 940 nm wavelengths (maximum power of 1.5 kW) and with optical fibre beam delivery system (with a spot area of 3.5 × 2 mm^2) using nitrogen as the shrouding gas. The scan speed was maintained at a constant 6 mm s^{-1}. The main process variables were laser power and gas flow rate. Following laser surface nitriding, the microstructures of the nitrided layer were characterized by scanning electron microscopy and transmission electron microscopy. The topographical features of the as-received and laser surface nitrided Ti–6Al–4V specimen surfaces were carried out using a scanning probe microscope (SPM) operated in atomic force microscopy tapping mode. A detailed analysis of the phase was carried out with an X-ray diffractometer. Residual stress introduced in the nitrided layer was measured by a stress goniometer attached to the X-ray diffractometer applying Cohen's theory [14]. Test works four software for a nanoindentation system was used to calculate the hardness and

* Corresponding author. Tel.: +91 3222 283288; fax: +91 3222 282280; e-mail: jyotsna@metal.iitkgp.ernet.in

1359-6462/$ - see front matter © 2008 Published by Elsevier Ltd. on behalf of Acta Materialia Inc.
doi:10.1016/j.scriptamat.2008.03.020

Table 1. Summary of optimum laser parameters for laser surface nitriding of Ti–6Al–4V and mechanical and electrochemical properties of the melt zone

Applied power, w (Gas flow rate, 1/min)	Micro-hardness (VHN)	Residual stress (MPa)	Young's modulus (GPa)	Average surface roughness R_a (μm)	Contact angle (°)	Critical potential for pit formation V(SCE)
700 (5)	912	−50	171	0.31	45 ± 1	1.88
800 (5)	897	−2450	173	0.30	41 ± 1	1.40
800 (10)	1102	−1250	177	0.29	48 ± 1	1.75
800 (20)	783	−1250	175	0.25	43 ± 1	1.80
As-received Ti–6Al–4V	280	50	115	0.044	60 ± 1	1.30

Young's modulus from a load–displacement graph using the Oliver and Pharr method [15]. Following the detailed correlation between the microstructures and properties of the nitrided surface with laser parameters, the optimum process parameters were established (cf. Table 1) [14]. In this regard, it is relevant to note that the optimum processing region corresponds to the laser parameters leading to the formation of a defect-free microstructure, with the introduction of compressive residual stress. The presence of macro/microcracks were the predominant defects in the microstructures, as reported earlier [16]. However, a detailed parametric correlation concerning the variation of defect densities with laser parameters was not undertaken in the present study.

Finally, the pitting corrosion behavior of the laser nitrided surface was compared with that of the as-received Ti–6Al–4V by calculating the corrosion rate derived from a potentiodynamic anodic polarization study in Hank's solution with the following electrolytic composition (g l^{-1}): 0.185 $CaCl_2$, 0.4 KCl, 0.06 KH_2PO_4, 0.1 $MgCl_2 \cdot 6H_2O$, 0.1 $MgSO_4 \cdot 7H_2O$, 8 NaCl, 0.35 $NaHCO_3$, 0.48 Na_2HPO_4 and 1.00 D-glucose. A standard calomel electrode was used as the reference electrode and platinum was used for the counter electrode [17]. The wettability of the laser nitrided surfaces were examined by the sessile-drop method [18] and compared with the as-received Ti–6Al–4V. The liquid drops contain a mixture of simulated body fluid (Hank's solution; SBF) and bovine serum albumin (BSA). The SBF has an inorganic ion concentration close to that found in human blood plasma. The BSA was dissolved in SBF at pH 7.40, at a concentration of 4 mg ml^{-1}.

Figure 1 shows the scanning electron micrograph of the top surface of laser gas nitrided Ti–6Al–4V lased with a power of 800 W and gas flow rate of 10 l min^{-1}. From Figure 1 it may be noted that laser surface nitriding causes the formation of a continuous and defect-free alloyed zone consisting of dendrites of titanium nitride (TiN) and α-Ti (as confirmed by X-ray diffraction analysis), with an average interdendritic spacing of 2–4 μm for different conditions of lasing. In this regard, it is relevant to mention that the distribution of nitrides in the melt zone was found to be almost uniform along the depth, possibly due to a convective flow developed during laser gas alloying. However, rapid solidification associated with laser processing limits the extent of gas alloying. The volume fraction of the titanium nitride phase and the interdendritic spacing were found to vary with the laser parameters. It was observed that the dendrites were marginally coarsened (with an increased secondary arm spacing) with increasing applied power. Earlier attempts on laser gas nitriding of Ti and its alloys using a CO_2 laser or an Nd:YAG laser also reported the presence of TiN dendrites [19–21].

Figure 2 shows a transmission electron micrograph of laser surface nitrided Ti–6Al–4V revealing the presence of nanocrystalline titanium nitride. The Moiré fringes (Fig. 2) found in the nitrided surface subdivide the grains into lamellae at a distance of about 25 nm. Moiré fringes should be formed by interference between two sets of lines that have near-identical periodicities. The Moiré pattern can often be thought of as a magnified view of the structure of the materials, such as the

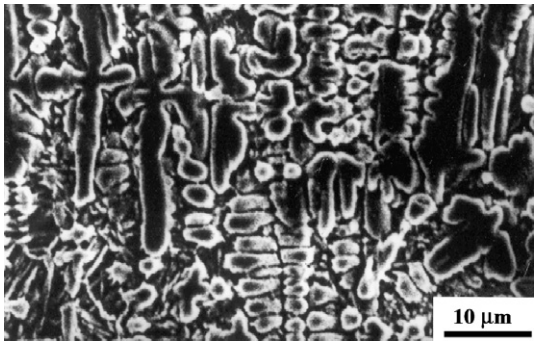

Figure 1. Scanning electron micrograph of the top surface of laser surface nitrided Ti–6Al–4V lased with a power of 800 W and gas flow rate of 10 l min^{-1}.

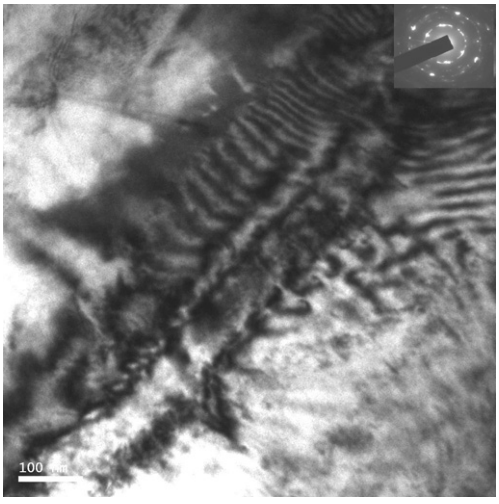

Figure 2. Transmission electron micrograph of the top surface of laser surface nitrided Ti–6Al–4V lased with a power of 800 W and gas flow rate of 10 l min^{-1}.

patterns used to locate and give information for dislocation. The SAED pattern of the sample shows diffraction rings that indicate the polycrystalline nature of the TiN.

The surface roughness of the nitrided layer was carefully measured from the surface topography analysis using an atomic force microscopy. Table 1 summarizes the average surface roughness of the as-received vs. the laser surface nitrided Ti–6Al–4V as a function of the laser parameters. From Table 1 it can be noted that there is a significant enhancement in surface roughness after surface nitriding (0.25–0.31 μm) as compared to the as-received Ti–6Al–4V (0.044 μm). The surface topography and the degree of surface roughness were, however, found to vary marginally with the laser parameters. It is well known that suitable surface roughness increases the adherence of cells above that of smooth surfaces [22]. Hence, the increase in the surface roughness following laser surface nitriding would be beneficial for improving biocompatibility. From Figure 3b it is also clear that the dendrite arm size of nitride was approximately 2–3 μm. Furthermore, a periodic microtexturing of the surface along a particular direction is also observed in laser surface nitrided Ti–6Al–4V, which varied from grain to grain. Table 1 summarizes the surface roughness as a function of the laser parameters (under optimum processing conditions) measured from the surface topography analysis.

The hardness distribution in the nitrided zone was carefully analyzed using the nanoindentation technique (by the application of a triangular pyramid (Berkovich) diamond indenter). Load–displacement data is the basic data acquired from the depth-sensing indentation system and reflects the loading–unloading history of the sample. The load–displacement plot observed by nanoindentation is substantially influenced by residual stress and the microstructure. General observations reveal that tensile residual stress tends to stretch out the load–displacement curves to larger depths, while compressive stress compresses the curves to smaller depths [23]. Figure 4 illustrates typical load–displacement curves for the as-received and laser surface nitrided Ti–6Al–4V indented with a maximum load of 500 mN. The curve is shifted left, suggesting that residual stress in this

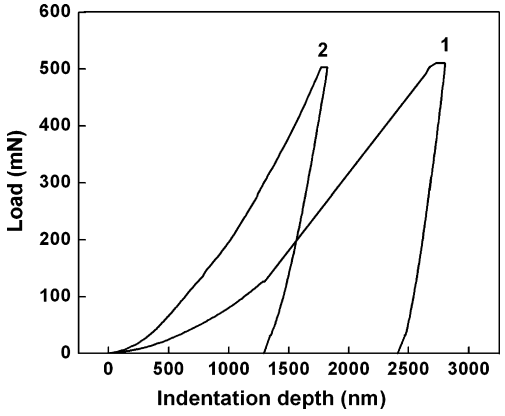

Figure 3. Load–displacement curves of as-received (plot 1) and laser surface nitrided (plot 2) (lased with a power of 800 W at a gas flow rate of 10 l min^{-1}) Ti–6Al–4V indented to a maximum load of 500 mN.

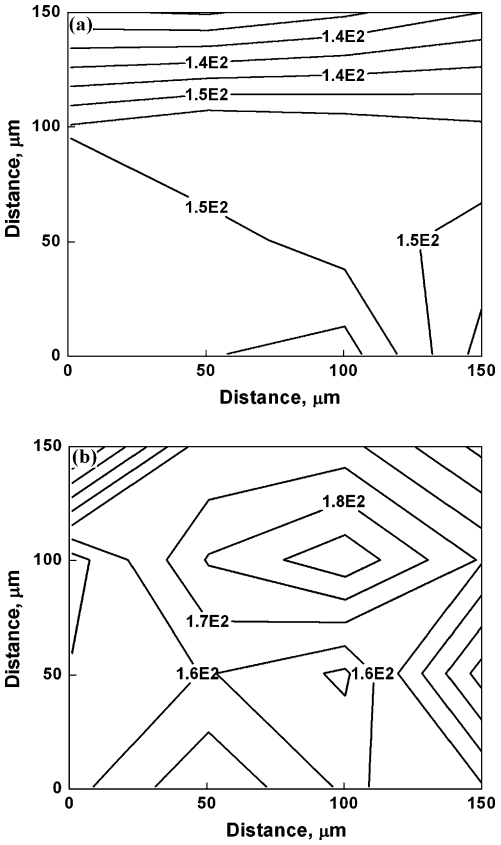

Figure 4. Iso-Young's modulous contour (in GPA) obtained from nanoindentation of (a) as-received and (b) laser surface nitrided (lased with a power of 800 W at a gas flow rate of 10 l min^{-1}) Ti–6Al–4V indented to a maximum load of 500 mN.

region is compressive, which is attributed to possibly stress generated during thermal quenching and may be due to the formation of TiN phase and supported by a detailed residual stress analysis by X-ray diffraction [14]. Table 1 summarizes the residual stress (evaluated by X-ray diffraction) developed on the surface nitrided Ti–6Al–4V lased under optimum process parameters. From Table 1 it may be noted that residual stress is mainly compressive in nature, with its magnitude varying from − 50 to −2450 MPa for different laser parameters. The introduction of residual compressive stress was attributed to the formation of titanium nitride in the microstructure. The magnitude of compressive residual stress on the surface was found to increase with increasing applied power and decreasing gas flow rate. Application of a low laser power and a high gas flow rate was found to introduce tensile residual stress on the surface nitrided zone. As the microstructure and nitride content were uniform throughout the microstructure, the determination of residual stress with depth was not evaluated in the present study. The microhardness of the nitrided zone is significantly increased to 600–1200 VHN as compared to the 280 VHN of as-received Ti–6Al–4V substrate (cf. Table 1). Kloosterman and De Hosson [24] reported the formation of a titanium nitride dispersed α-Ti matrix surface with an average microhardness ranging from 700 to 1800 VHN following laser gas nitriding of cp-titanium. However,

cracking was a commonly encountered problem in the nitrided zone, due to the presence of residual tensile stress on the surface. A similar study by Mridha and Baker [16] also reported an improved hardness (to a value of 1480 VHN) by laser gas nitriding of Ti using a continuous wave CO_2 laser with the presence of cracks. In the present study, defect formation was completely avoided under optimum laser parameters.

Figure 4a and b shows iso-Young's modulus contours obtained from nanoindentation of (a) as-received and (b) laser surface nitrided (lased with a power of 800 W and gas flow rate of 10 l min^{-1}) Ti–6Al–4V. From Figure 4b it may be noted that the Young's modulus distribution is almost uniform, with an average value of 177 GPa in laser surface nitrided Ti–6Al–4V. A close comparison between Figure 4a and b shows that the Young's modulus is increased due to laser surface nitriding compared to as-received Ti–6Al–4V (114 Gpa). The average Young's modulus of the nitrided surface was found not to vary with laser parameters (cf. Table 1). In this regard, it is relevant to note that the Young's modulus of TiN thin films has been widely studied, but the values cover a relatively wide range, between 100 and 600 GPa, based on the deposition techniques and deposition parameters [25]. The difference in Young's modulus was attributed to variable coating quality resulting from different nitrogen concentrations and porosity. It has previously been reported that the modulus increased steadily with nitrogen content and reached a maximum around the stoichiometric composition [25]. On the other hand, the reported Young modulus of the bulk sintered TiN component was reported to be 430.8 GPa [26]. A significantly lower Young's modulus of the laser surface nitrided Ti–6Al–4V as compared to the bulk sintered TiN is attributed to the development of a titanium nitride dispersed α-Ti composite surface layer rather than a continuous and monolithic titanium nitride layer.

Table 1 summarizes the measured potential for pit formation (E_{pp1}) and the contact angle of SBF on the surface for as-received vs. laser surface nitrided Ti–6Al–4V processed under optimum parameters. It is interesting to note that measured pitting potential (E_{pp1}) of the nitrided surface (in a Hank's solution) increases significantly as compared to as-received Ti–6Al–4V. Increased pitting potential due to laser surface nitriding is due to the presence of TiN on the surface and the presence of nitrogen in solution. The contact angle of SBF on the surface nitrided Ti–6Al–4V layer is significantly reduced to 41–47° as compared to 60° in as-received Ti–6Al–4V (cf. Table 1). The decrease in the contact angle is an indication of increased wettability. The reason behind the increased wettability is possibly the increase in surface roughness, and also the microstructural changes wrought by the laser surface nitriding.

From the above-mentioned investigations, it may be concluded that this is a first attempt at laser surface nitriding Ti–6Al–4V with a continuous wave diode laser to form a defect-free nitride zone. The microstructure of the nitride layer consists of TiN dendrites in α-Ti matrix with improved microhardness (to 600–1200 VHN) as compared to the as-received Ti–6Al–4V substrate (280 VHN). The average bulk modulus of the nitride dispersed layer was increased to 177 GPA as compared to the 114 GPA of the as-received Ti–6Al–4V. The pitting corrosion resistance is significantly improved by laser surface nitriding. This is the first time that the contact angle of SBF against surface nitrided Ti–6Al–4V has been reported to be significantly reduced (41–48°) as compared to as-received Ti–6Al–4V (60°), and this is attributed to the improved surface roughness. Hence, it can be concluded that the proposed gas nitriding of Ti–6Al–4V can be usefully applied to bioimplant surfaces.

The financial support for this work from the Council of Scientific and Industrial Research (CSIR) and Department of Science and Technology (DST), N. Delhi and the Board of Research on Nuclear Science (BRNS), Bombay is gratefully acknowledged.

[1] J. Probst, U. Gbureck, R. Thull, Surf. Coat. Technol. 148 (2001) 226.
[2] E.I. Meletis, C.V. Cooper, K. Marchev, Surf. Coat. Technol. 113 (1999) 201.
[3] S. Fukumoto, H. Tsubakino, S. Inoue, L. Liu, M. Terasawa, T. Mitamura, Mater. Sci. Eng. A 263 (1999) 205.
[4] R.R. Wang, G.E. Welsch, O. Monteiro, J. Biomed. Mater. Res. 46 (1999) 262.
[5] M.C. Kuo, S.K. Yen, Mater. Sci. Eng. C 20 (2002) 153.
[6] E.S. Thian, K.A. Khor, N.H. Loh, S.B. Tor, Biomaterials 22 (2001) 1225.
[7] A.K. Lynn, D.L. DuQuesnay, Biomaterials 23 (2002) 1937.
[8] J. Dutta Majumdar, I. Manna, Sadhana 28 (2003) 495.
[9] B.L. Mordike, Prog. Mater. Sci. 42 (1997) 357.
[10] T. Bell, H.W. Bergmann, J. Lanagan, P.H. Morton, A.M. Staines, J. Surf. Eng. 2 (1986) 133.
[11] J.M. Robinson, B.A. Van Brussel, J.Th.M.De. Hosson, R.C. Reed, J. Mater. Sci. A 204 (1996) 143.
[12] H.C. Man, Z.D. Cui, X.J. Yang, Appl. Surf. Sci. 199 (2002) 293.
[13] A. Biswas, L. Li, T.K. Maity, U.K. Chatterjee, I. Manna, J. Dutta Majumdar, Laser. Eng. 20 (2006) 68.
[14] B.D. Cullity, S.R. Stock, Elements of X-Ray Diffraction, 3rd ed., Prentice Hall, New Delhi, 2001, p. 435.
[15] W.C. Oliver, G.M. Pharr, J. Mater. Res. 7 (1992) 1564.
[16] S. Mridha, T.N. Baker, J. Mater. Process. Technol. 77 (1998) 115.
[17] M.G. Fontana, Corrosion Engineering, McGraw-Hill, New York, 1987, p. 71.
[18] A.W. Adamson, Physical Chemistry of Surface, John Wiley, New York, 1990, p. 298.
[19] H.C. Man, N.Q. Zhao, Z.D. Cui, Surf. Coat. Technol. 192 (2005) 341.
[20] X. Chen, G. Wu, R. Wang, W. Guo, J. Yang, S. Cao, Y. Wang, W. Han, Surf. Coat. Technol. 201 (2007) 4843.
[21] B.S. Yilbas, C. Karatas, U.O. Keles, I.Y. Usta, M. Ahsan, Appl. Surf. Sci. 252 (2006) 8557.
[22] J.A. Helsen, H.J. Breme, Metals as Biomaterials, John Willey & Sons, New York, 1998, p.153.
[23] J.G. Swadener, B. Taljat, G.M. Pharr, J. Mater. Res. 16 (2001) 2091.
[24] A.B. Kloosterman, J.Th.M. De Hosson, Scripta Metall. et Mater. 33 (1995) 567.
[25] E. ToÈroÈk, A.J. Perry, L. Cholet, W.D. Sproul, Thin Solid Films 153 (1987) 37.
[26] H. Kuwahara, N. Mazaki, M. Takahashi, T. Watanabe, X. Yang, T. Aizaw, Mater. Sci. Eng. A 319–321 (2001) 687.